

Supplementary Materials to paper

Structure and properties of heterometallics based on lanthanides and transition metals with methoxy- β -diketonates

Vladislav V. Krisyuk¹, Samara Urkasym kyzy¹, Tatyana V. Rybalova², Ilya V. Korolkov¹, Mariya A. Grebenkina^{1,3} and Alexander .N. Lavrov^{1*}

¹ Nikolaev Institute of Inorganic Chemistry, SB RAS, Lavrentiev Ave. 3, 630090 Novosibirsk, Russia; kvv@niic.nsc.ru (V.V.K.)

² Vorozhtsov Novosibirsk Institute of Organic Chemistry SB RAS, Lavrentiev Ave. 9, 630090 Novosibirsk, Russia

³ Novosibirsk National Research State University, 1 Pirogova Str., 630090 Novosibirsk, Russia

* Correspondence: lavrov@niic.nsc.ru (A.N.L.), kvv@niic.nsc.ru (V.V.K.)

Content

Table S1: XRD data for complexes **1,2,5,6,8,9**.

Figure S1: A view of the cell packing along Z axis in crystals of **2**.

Figure S2: XRD data for solid residue after sintering $[(La(L^1)_2tmhd)_2Cu(tmhd)_2]$ in comparison with appropriate PDF files.

Figure S3: XRD data for solid residue after sintering $[(La(L^1)_2tmhd)_2Co(tmhd)_2]$ in comparison with appropriate PDF files.

Figure S4: XRD data for solid residue after sintering $[(La(L^1)_2tmhd)_2Ni(tmhd)_2]$ in comparison with appropriate PDF files.

Figure S5: XRD data for solid residue after sintering $[(La(L^1)_2tmhd)_2Mn(tmhd)_2]$ in comparison with appropriate PDF files.

Results of magnetic measurements for the heterocomplexes

Gd-Cu complex (**4**)

Figure S6: (a) Temperature dependence of the magnetic susceptibility χ measured for the Gd-Cu complex at the magnetic field $H=1$ kOe. (b) Temperature dependences of μ_{eff} and $1/\chi p$. The depicted effective moment μ_{eff} is calculated for the case of non-interacting magnetic moments ($\theta = 0$).

Pr-Cu complex (**2**)

Figure S7: (a) Temperature dependence of the magnetic susceptibility χ measured for the Pr-Cu complex at the magnetic fields $H = 1; 10$ kOe. (b) Temperature dependences of μ_{eff} and $1/\chi p$. The depicted effective moment μ_{eff} is calculated for the case of non-interacting magnetic moments ($\theta = 0$).

Sm-Cu complex (**3**)

Figure S8: (a) Temperature dependence of the magnetic susceptibility χ measured for the Sm-Cu complex at the magnetic fields $H = 1; 10$ kOe. (b) Temperature dependences of μ_{eff} and $1/\chi p$. The depicted effective moment μ_{eff} is calculated for the case of non-interacting magnetic moments ($\theta = 0$).

La-Co complex (**5**)

Figure S9: (a) Temperature dependence of the magnetic susceptibility χ measured for the La-Co complex at the magnetic fields $H = 1; 10$ kOe. (b) Temperature dependences of μ_{eff} and $1/\chi p$. The depicted effective moment μ_{eff} is calculated for the case of non-interacting magnetic moments ($\theta = 0$). (c) Magnetic field dependence of the magnetization measured at $T = 1.77$ K.

La-Ni complex (**6**)

Figure S10: (a) Temperature dependence of the magnetic susceptibility χ measured for the La-Ni complex at the magnetic fields $H = 1; 10$ kOe. (b) Temperature dependences of μ_{eff} and $1/\chi p$. The depicted effective moment μ_{eff} is calculated for the case of non-interacting magnetic moments ($\theta = 0$).

Table S1: XRD data for complexes **1,2,5,6,8,9**.

Compound	1	2	5	6	8	9
Empirical formula	C ₇₂ H ₁₀₈ F ₁₂ O ₂₄ CuLa ₂	C ₇₂ H ₁₀₈ F ₁₂ O ₂₄ CuPr ₂	C ₇₂ H ₁₀₈ CoF ₁₂ La ₂ O ₂₄	C ₇₂ H ₁₀₈ F ₁₂ La ₂ NiO ₂₄	C ₇₆ H ₁₁₆ CuF ₁₂ La ₂ O ₂₄	C ₄₈ H ₆₀ F ₁₈ La ₂ O ₁₈
Formula weight	1926.94	1930.95	1922.33	1922.11	1983.04	1544.78
	200(2) K	200(2) K	150(2) K	150(2) K	150(2) K	110(2) K
Wavelength Å	0.71073	0.71073	0.71073	0.71073	0.71073	0.71073
Crystal system	Monoclinic	Monoclinic	Monoclinic	Monoclinic	Monoclinic	Monoclinic
Space group	P2(1)/n	P2(1)/n	<i>P2₁/n</i>	<i>P2₁/n</i>	<i>P2₁/n</i>	<i>P2₁/c</i>
Unit cell dimensions <i>a</i> , Å	13.0379(8)	13.0009(6)	13.0328(4)	13.0158 (7)	12.8652(5)	18.2778(4)
<i>b</i> , Å	21.985(1)	21.9732(1)	21.964(1)	21.993(2)	22.5354(9)	19.9517(3)
<i>c</i> , Å	15.0964(8)	15.0612(6)	14.6846(6)	14.5878(8)	15.2704(6)	16.7143(3)
α , °	90	90	90	90	90	90
β , °	97.289(2)	97.354(2)	96.803 (1)	96.719 (2)	95.940 (2)	97.888 (1)
γ , °	90	90	90	90	90	90
Volume, Å ³	4292.1(4)	4267.2(3)	4173.8 (3)	4147.2 (4)	4403.5 (3)	6037.58 (19)
Z	2	2	2	2	2	4
Density (calcd.), Mg.m ⁻³	1.491	1.503	1.530	1.539	1.496	1.699
Abs. coefficient, mm ⁻¹	1.317	1.466	1.30	1.33	1.29	1.52
F(000)	1966	1974	1962	1964	2030	3072
Crystal size, mm ³	0.32 × 0.08 × 0.03	0.57 × 0.11 × 0.05	0.25 × 0.08 × 0.04	0.26 × 0.22 × 0.05	0.12 × 0.1 × 0.09	0.29 × 0.16 × 0.14
Θ range for data collection, °	2.7 – 29.4	2.3 – 34.4	2.3 - 25.8	1.8 - 27.1	2.2 - 31.6	1.5 - 29.6
Index ranges	-18 ≤ <i>h</i> ≤ 18, -30 ≤ <i>k</i> ≤ 30, -20 ≤ <i>l</i> ≤ 20	-20 ≤ <i>h</i> ≤ 20, -34 ≤ <i>k</i> ≤ 34, -23 ≤ <i>l</i> ≤ 22	-11 ≤ <i>h</i> ≤ 15, -17 ≤ <i>k</i> ≤ 26, -17 ≤ <i>l</i> ≤ 17	-16 ≤ <i>h</i> ≤ 12, -26 ≤ <i>k</i> ≤ 28, -18 ≤ <i>l</i> ≤ 18	-18 ≤ <i>h</i> ≤ 18, -33 ≤ <i>k</i> ≤ 33, -22 ≤ <i>l</i> ≤ 22	-22 ≤ <i>h</i> ≤ 25, -24 ≤ <i>k</i> ≤ 27, -23 ≤ <i>l</i> ≤ 20

Reflections collected	94240	115128	20278	34638	209635	49738
Independent reflections	11842 [R(int) 0.049]	17896 [R(int) 0.047]	7937 [R(int) 0.028]	9149 [R(int) 0.159]	14670 [R(int) 0.057]	16948 [R(int) 0.044]
Reflections $I > 2\sigma(I)$	9599	14502	6584	6009	12323	12912
Completeness to θ %	99.7, $\theta = 25.25^\circ$	99.9, $\theta = 25.25^\circ$	99.5, $\theta = 25.25^\circ$	100, $\theta = 25.25^\circ$	99.9, $\theta = 25.25^\circ$	99.8, $\theta = 25.25^\circ$
parameters / restraints	572/ 30	584/ 23	547 / 24	518 / 0	620 /79	834 / 6
Max. and min. transmission	0.678, 0.962	0.489, 0.930	0.615, 0.745	0.651, 0.746	0.679, 0.746	0.664, 0.746
Refinement method	Full matrix LSM against F^2	Full matrix LSM against F^2	Full matrix LSM against F^2	Full matrix LSM against F^2	Full matrix LSM against F^2	Full matrix LSM against F^2
Goodness-of-fit on $L4$	1.068	1.294	1.02	0.98	1.07	1.01
Final R indices $I > 2\sigma(I)$: R_1 , wR_2	0.0333, 0.0857	0.0491, 0.1249	0.038, 0.1069	0.039, 0.085	0.046, 0.113	0.035, 0.064
Final R indices (all data): R_1 , wR_2	0.0511, 0.1003	0.0696, 0.1368	0.0511, 0.115	0.1016, 0.097	0.057, 0.120	0.056, 0.072
Largest diff. peak / hole, $e.\text{\AA}^{-3}$	1.03 / -0.87	2.29 / -1.02	0.83, -0.68	1.31, -1.54	1.60, -1.33	0.68, -0.69
*CCDC deposition numbers	1534092	1534091	2175224	2175225	2175226	2175227

* Cif-files can be obtained free of charge from The Cambridge Crystallographic Data Centre via www.ccdc.cam.ac.uk/data_request/cif

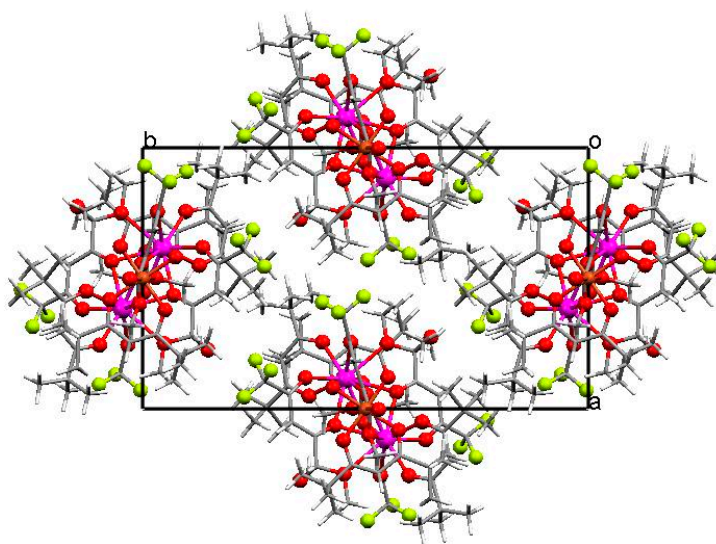


Figure S1: A view of the cell packing along Z axis in crystals of **2**.

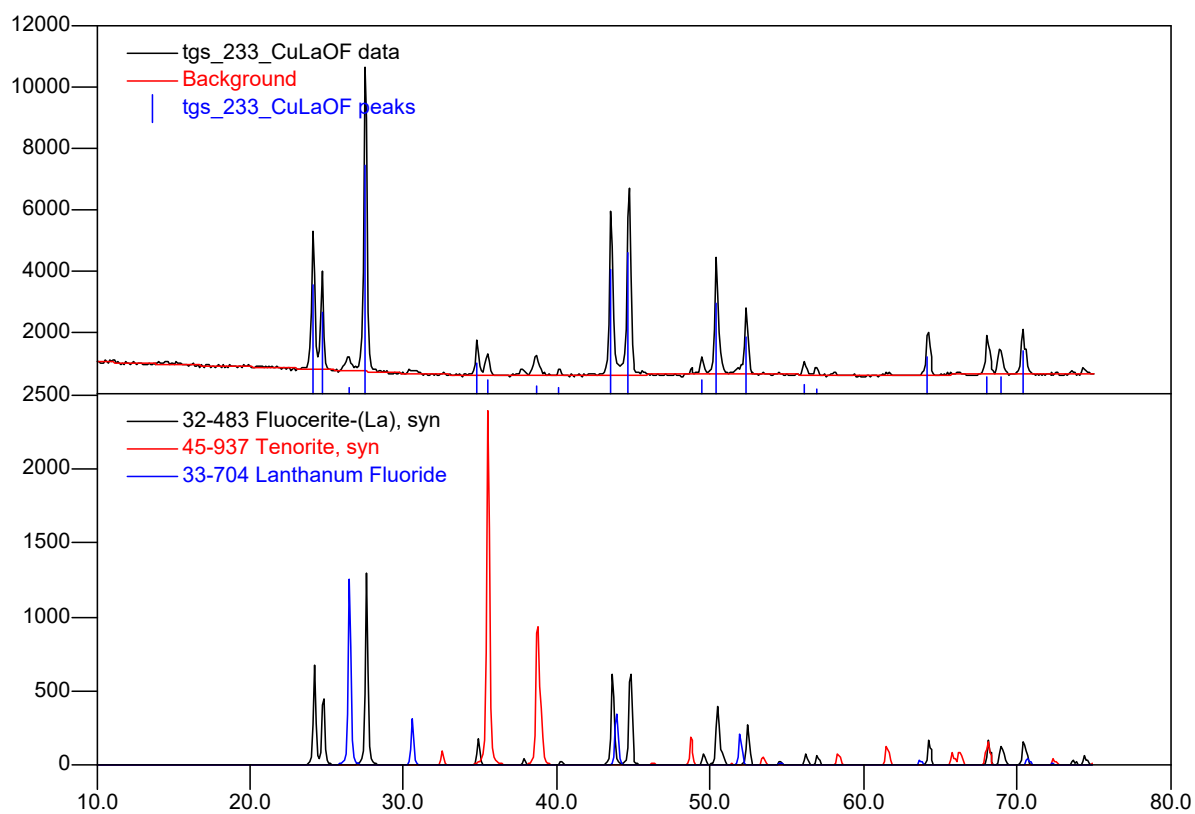


Figure S2: XRD data for solid residue after sintering $[(\text{La}(\text{L}^1)_2\text{tmhd})_2\text{Cu}(\text{tmhd})_2]$ in comparison with appropriate PDF files.

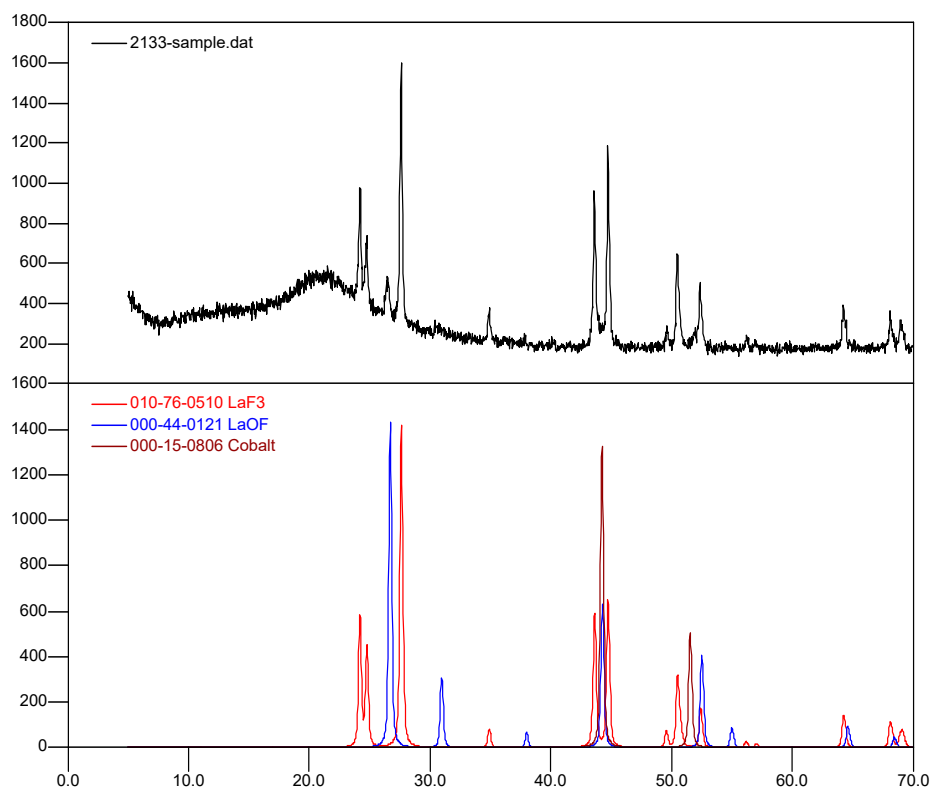


Figure S3: XRD data for solid residue after sintering $[(\text{La}(\text{L}^1)_2\text{tmhd})_2\text{Co}(\text{tmhd})_2]$ in comparison with appropriate PDF files

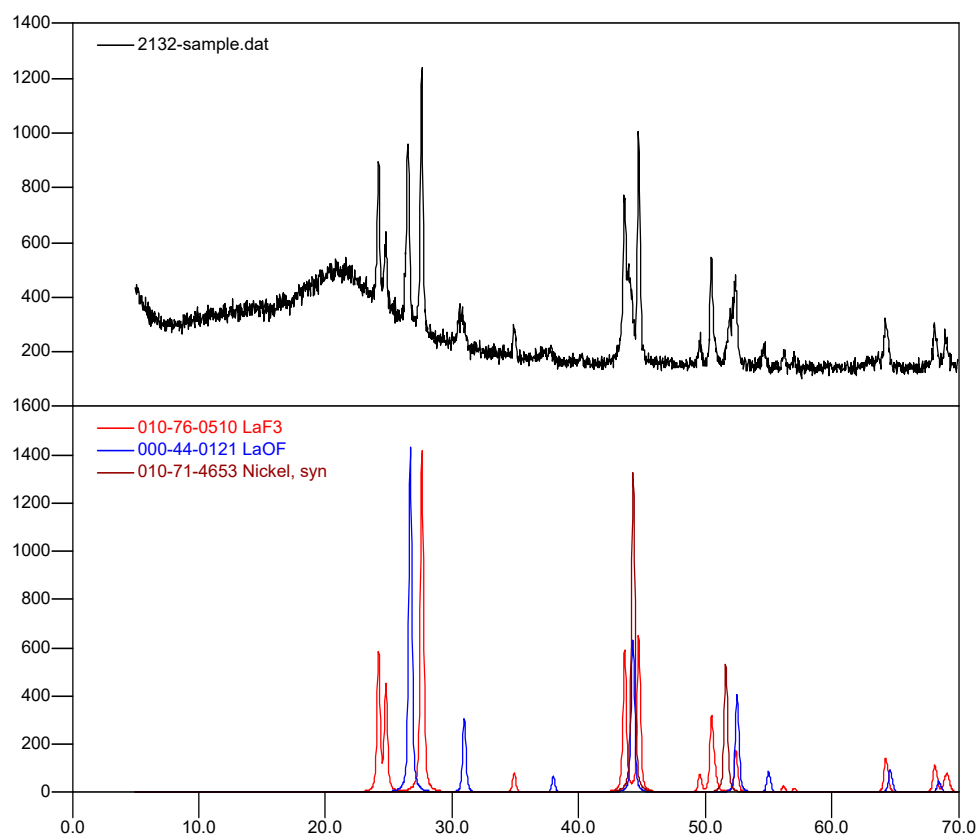


Figure S4: XRD data for solid residue after sintering $[(\text{La}(\text{L}^1)_2\text{tmhd})_2\text{Ni}(\text{tmhd})_2]$ in comparison with appropriate PDF files.

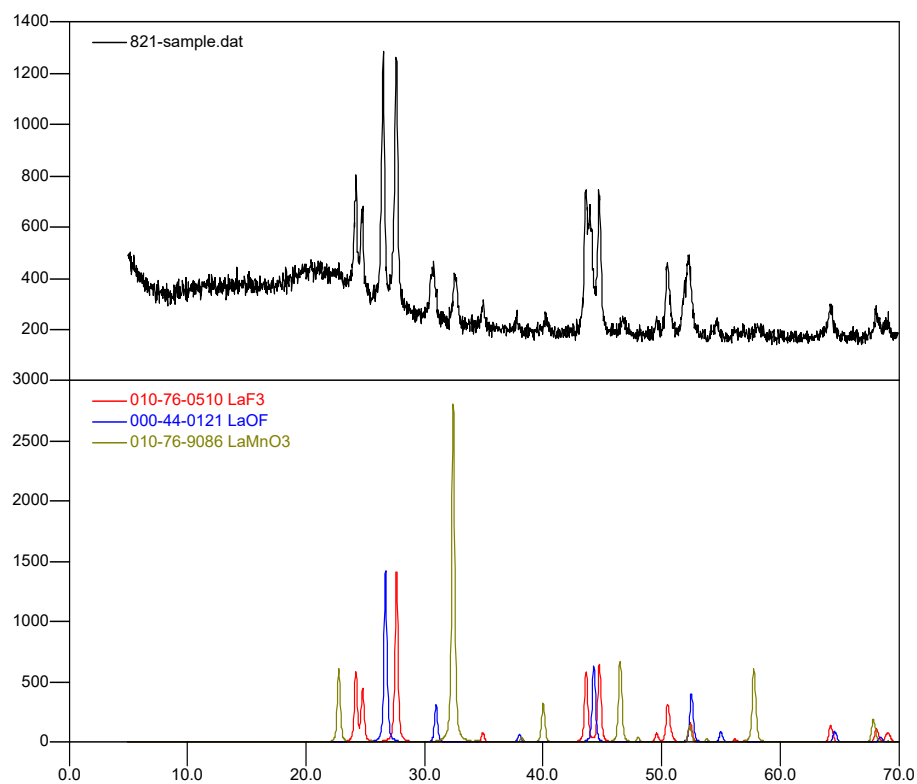


Figure S5: XRD data for solid residue after sintering $[(\text{La}(\text{L}^1)_2\text{tmhd})_2\text{Mn}(\text{tmhd})_2]$ in comparison with appropriate PDF files.

Results of magnetic measurements for the heterocomplexes

Gd-Cu complex (4)

The Gd-Cu complex is found to exhibit paramagnetic behavior throughout the available temperature range without any magnetic phase transition (Figure S6a). The paramagnetic behavior can be well described by the Curie-Weiss dependence $\chi_p(T) = N_A \mu_{\text{eff}}^2 / 3k_B(T - \theta)$ with a nearly zero Weiss constant $\theta \approx -0.4$ K (Figure S6b). At high temperatures, the measured effective magnetic moment $\mu_{\text{eff}} \sim 11.47 \mu_B$ corresponds very well to the values expected for two gadolinium ions Gd^{3+} , $\mu_{\text{eff}}(\text{Gd}) \approx 7.94 \mu_B$, and one copper ion Cu^{2+} , $\mu_{\text{eff}}(\text{Cu}) \approx 2 \mu_B$: $\mu_{\text{eff}} \approx \sqrt{2 \cdot 7.94^2 + 2^2} \approx 11.41 \mu_B$. In the low-temperature region, the $1/\chi_p(T)$ dependence deviates from linearity and the calculated effective magnetic moment decreases slightly both due to the nonlinearity of the magnetization curve expected for Gd^{3+} ions ($S = 7/2$) in the region of fields $g\mu_B SH \sim k_B T$ and a very weak inter-ion exchange or dipole-dipole interactions. Thus, the studied compound can be considered as a set of virtually non-interacting gadolinium Gd^{3+} ions ($S = 7/2$) and Cu^{2+} ions ($S = 1/2$).

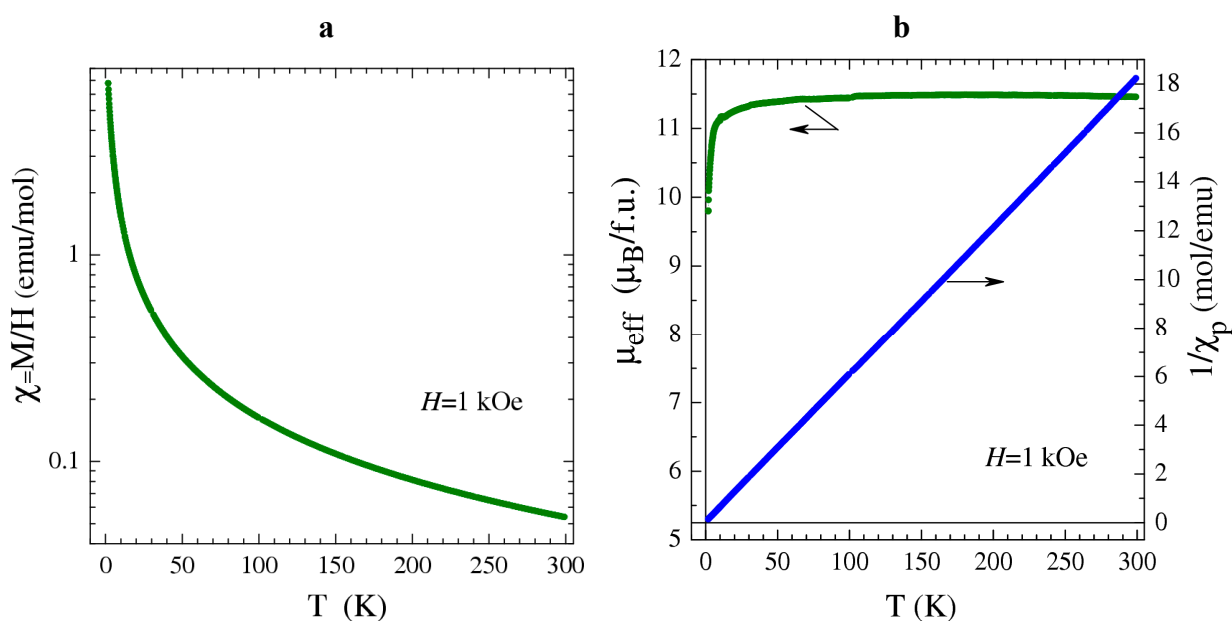


Figure S6: (a) Temperature dependence of the magnetic susceptibility χ measured for the Gd-Cu complex at the magnetic field $H=1$ kOe. (b) Temperature dependences of μ_{eff} and $1/\chi_p$. The depicted effective moment μ_{eff} is calculated for the case of non-interacting magnetic moments ($\theta = 0$).

Pr-Cu complex (2)

The Pr-Cu complex exhibits paramagnetic behavior throughout the available temperature range with a low-temperature peculiarity that at a first glance looks like a manifestation of inter-ion interactions (Figure S7a); on the $\chi(T)$ plot, it seems that the susceptibility begins to grow faster at $T < 7-8$ K. However, in fact it is the low-temperature region where the susceptibility behavior matches the Curie-Weiss dependence with the Weiss constant θ close to zero (Figure S7b), while at higher temperatures the susceptibility behavior is determined by the changes in effective moment μ_{eff} . In the highest temperature region of 200-300 K, the $\chi_p(T)$ data can be described by the Curie-Weiss dependence with an effective magnetic moment $\mu_{\text{eff}} \approx 5.38 \mu_B$ (Figure S2b), which agrees well with the value expected for two Pr^{3+} ions ($S = 1$, $L = 5$, $J = 4$) and one Cu^{2+} ion ($S = 1/2$, $g = 2.1$): $\mu_{\text{eff}} \approx \sqrt{2 \cdot 3.58^2 + 1.82^2} \approx 5.38 \mu_B$. On cooling, the effective magnetic moment decreases down to $\mu_{\text{eff}} \approx 2.07 \mu_B$ at $T = 1.77$ K. This decrease corresponds in magnitude to the complete disappearance of the contribution from the praseodymium ions while the contribution from Cu^{2+} ions is kept intact. Since the disappearance of the magnetic contribution of Pr^{3+} ions as a result of their antiferromagnetic (AFM) interaction requires unrealistically strong exchange interactions, the most likely explanation is the singlet ground state of each Pr^{3+} ion, a state quite common for Pr^{3+} ions, for instance, in hexagonal or cubic environment [*1]. Consequently, at low temperatures the magnetic susceptibility of the Pr-Cu complex is predominantly determined by Cu^{2+} ions, while at higher temperatures the contribution from excited levels of the Pr^{3+} ion multiplet is added.

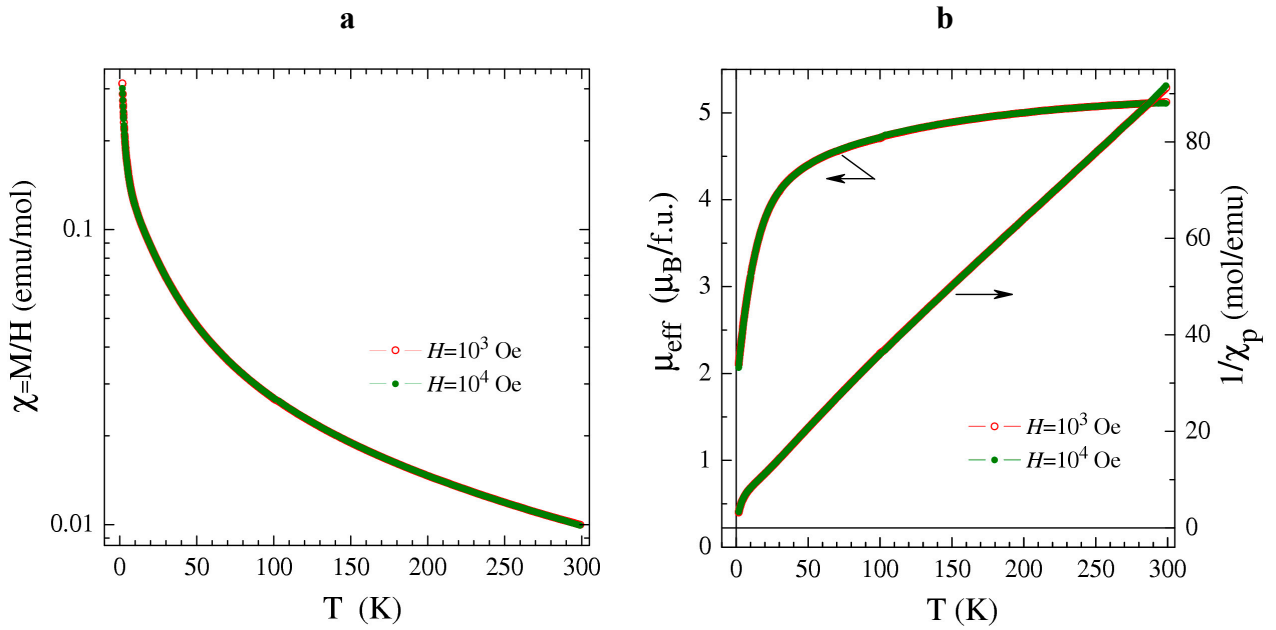


Figure S7: (a) Temperature dependence of the magnetic susceptibility χ measured for the Pr-Cu complex at the magnetic fields $H = 1; 10$ kOe. (b) Temperature dependences of μ_{eff} and $1/\chi_p$. The depicted effective moment μ_{eff} is calculated for the case of non-interacting magnetic moments ($\theta = 0$).

Sm-Cu complex (3)

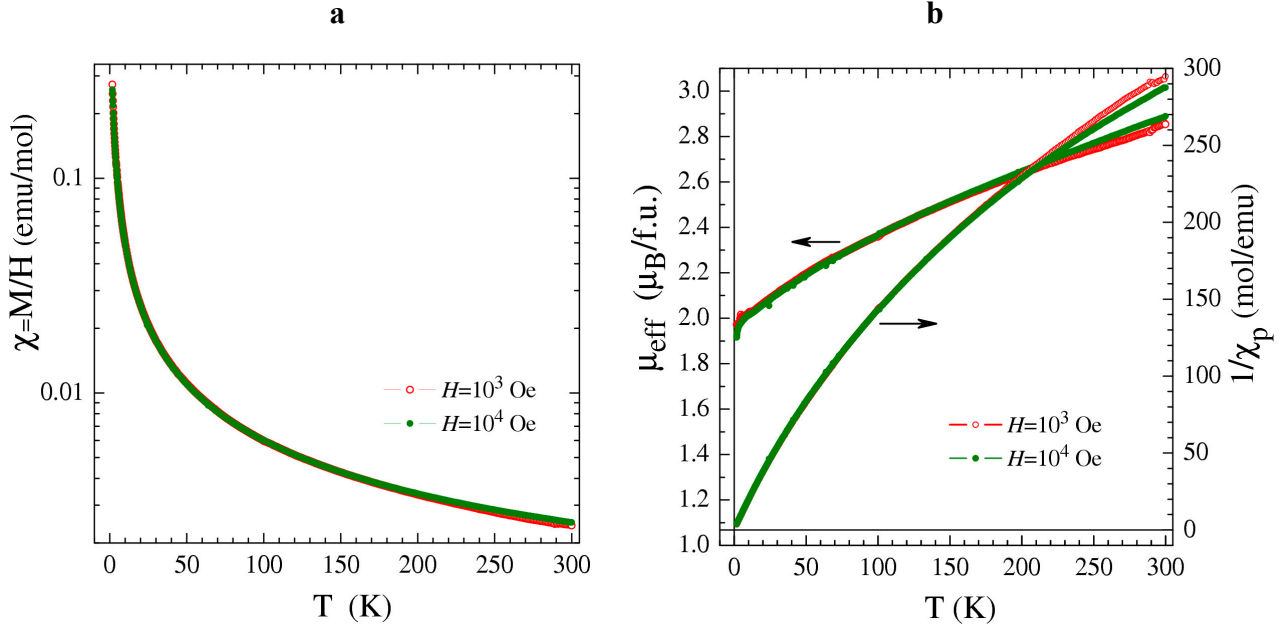


Figure S8: (a) Temperature dependence of the magnetic susceptibility χ measured for the Sm-Cu complex at the magnetic fields $H = 1; 10$ kOe. (b) Temperature dependences of μ_{eff} and $1/\chi_p$. The depicted effective moment μ_{eff} is calculated for the case of non-interacting magnetic moments ($\theta = 0$).

The Sm-Cu complex demonstrates paramagnetic behavior throughout the available temperature range (Figure S8a) without any noticeable sign of inter-ion interactions. The latter is confirmed by the fact that the $1/\chi_p$ curve goes exactly to the origin and the $\mu_{\text{eff}}(T)$ dependence does not exhibit any singularity upon approaching $T = 0$ (Figure S8b). The effective moment calculated for the case of non-interacting ions ($\theta = 0$) reaches $\mu_{\text{eff}} \approx 2.87 \mu_B$ at room temperature (Figure S8b), which agrees well with the values observed usually for samarium Sm^{3+} ions, $\mu_{\text{eff}}(\text{Sm}) \approx 1.5 \mu_B$, and copper Cu^{2+} , $\mu_{\text{eff}}(\text{Cu}) \approx 2 \mu_B$: $\mu_{\text{eff}} \approx \sqrt{2 \cdot 1.5^2 + 2^2} \approx 2.92 \mu_B$. As the temperature decreases, μ_{eff} decreases smoothly from $\sim 2.87 \mu_B$ down to $\sim 2.0 \mu_B$ at $T = 1.77$ K. Most likely, the effective-moment reduction originates from the transition of Sm^{3+} ions to the doublet $\pm 1/2$ ground state which is weakly magnetic due to the small g factor. Consequently, the magnetic susceptibility of the Sm-Cu complex at low temperature is determined mainly by the contribution of Cu^{2+} ions with a small addition from Sm^{3+} ones, while at higher temperatures excited doublets of the Sm^{3+} ground-state multiplet $J = 5/2$ as well as levels of other multiplets come into play resulting in the increase of the Sm^{3+} contribution [*1].

La-Co complex (5)

The La-Co complex exhibits paramagnetic behavior throughout the available temperature range without any magnetic phase transition or manifestation of inter-ion interactions (Figure S9a). The absence of significant inter-ion interactions is confirmed by the $1/\chi_p$ curve tending to zero at $T \approx 0$ and the $\mu_{\text{eff}}(T)$ dependence approaching zero temperature without singularity (Figure S9b). The effective magnetic moment measured in the field $H = 1$ kOe varies from $\mu_{\text{eff}} \approx 4.73 \mu_B$ at room temperature to $\mu_{\text{eff}} \approx 3.8 \mu_B$ at $T = 1.77$ K. Both high- and low-temperature μ_{eff} values are typical of Co^{2+} ($S = 3/2$) complexes. At high temperature, μ_{eff} significantly exceeds the theoretical spin-only value of $3.87 \mu_B$ due to the contribution of orbital moments. At low temperature, the effective magnetic momentum decreases both due to the reduction of the orbital-moment contribution and as a result of zero-field splitting of the Co^{2+} multiplet by the crystal field [*2]. It should be noted that the sharp drop in μ_{eff} measured in the field $H = 10$ kOe seen at low temperatures is not a manifestation of exchange interactions but is caused by the nonlinearity of the magnetization $M(H)$ curve, typical for Co^{2+} ions ($S = 3/2$) (Figure S9c). Thus, from the point of view of magnetic properties the La-Co complex can be considered as a set of almost non-interacting Co^{2+} ions ($S = 3/2$).

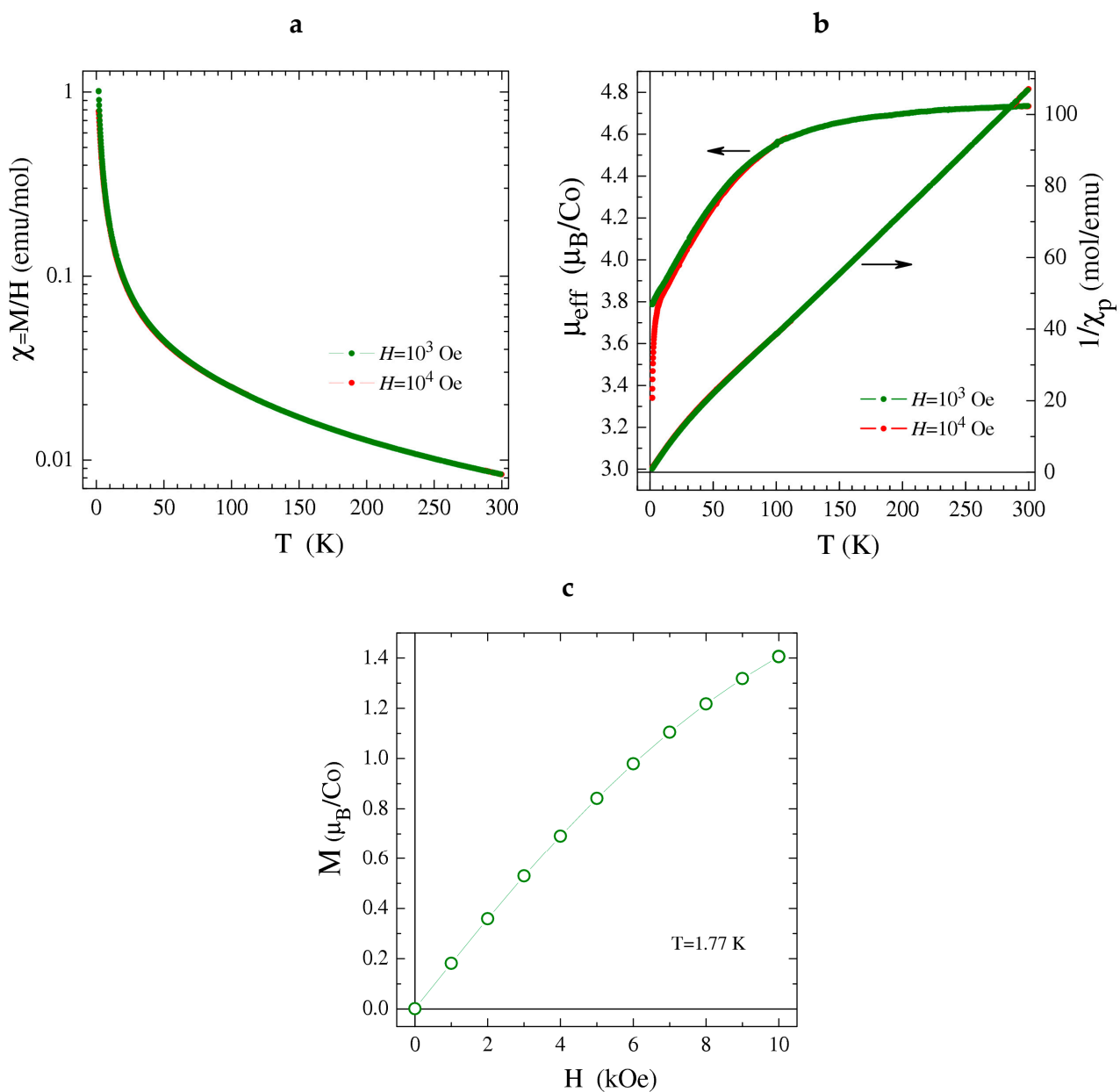


Figure S9: (a) Temperature dependence of the magnetic susceptibility χ measured for the La-Co complex at the magnetic fields $H = 1$; 10 kOe. (b) Temperature dependences of μ_{eff} and $1/\chi_p$. The depicted effective moment μ_{eff} is calculated for the case of non-interacting magnetic moments ($\theta = 0$). (c) Magnetic field dependence of the magnetization measured at $T = 1.77$ K.

La-Ni complex (6)

The La-Ni complex exhibits paramagnetic behavior throughout the available temperature range (Figure S10), but at the lowest temperatures the paramagnetic susceptibility growth slows noticeably, indicating a transition to a weakly magnetic state. The calculated effective magnetic moment decreases smoothly from $\mu_{\text{eff}} \approx 3.15 \mu_{\text{B}}$ at room temperature down to $\mu_{\text{eff}} \approx 1.1 \mu_{\text{B}}$ at $T = 50$ K. The high-temperature value of μ_{eff} is close to the theoretical spin-only value of $2.83 \mu_{\text{B}}$ for Ni^{2+} ($S = 1$); the slight excess is due to the contribution of orbital moments. The smooth decrease of the effective moment upon cooling is associated with the transition of Ni^{2+} ions into the weakly magnetic (singlet) ground state as a result of zero-field splitting of the $S = 1$ multiplet [*2] or formation of the low-spin $S = 0$ state.

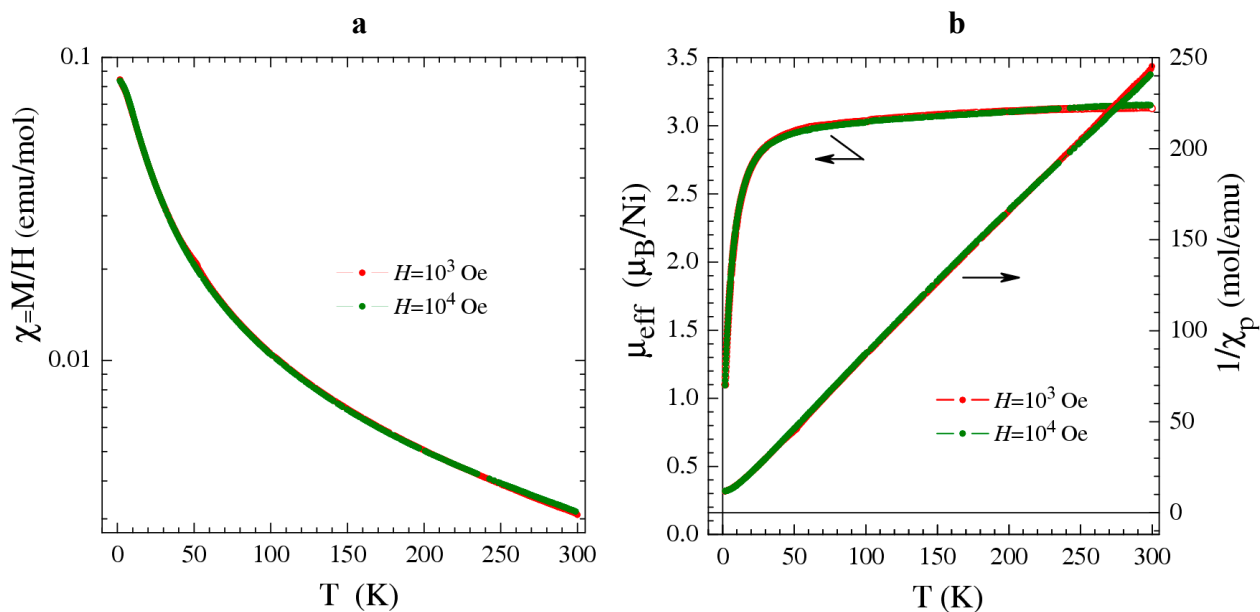


Figure S10: (a) Temperature dependence of the magnetic susceptibility χ measured for the La-Ni complex at the magnetic fields $H = 1; 10$ kOe. (b) Temperature dependences of μ_{eff} and $1/\chi_p$. The depicted effective moment μ_{eff} is calculated for the case of non-interacting magnetic moments ($\theta = 0$).

[*1] A. K. Zvezdin, V. M. Matveev, A. A. Mukhin, and A. I. Popov, *Rare Earth Ions in Magnetically Ordered Crystals* (Nauka, Moscow, 1985).

[*2] R. Boča, *Coord. Chem. Rev.* **248**, 757 (2004).